Supplementary materials

List of contents

Section 1: Details of catchment properties

Table S1-2: Tables showing data of sampling locations and various catchment parameters.

5 Section 2: Details of preheat plateau and dose recovery test

- Table S3: Protocol used for dose recovery tests on multi-grain and single-grain.
- Table S4: Preheat and post-IR IRSL stimulation temperature combinations.
- Fig. S1: Results of multi-grain dose recovery and residual preheat plateau test.
- Fig. S2: Results of single-grain dose recovery test.
- 10 Fig. S3: KDE plot of all four samples subjected to the single-grain dose recovery test.

Section 3: Details of ancillary luminescence data

- Fig. S4: Luminescence decay and dose response curves.
- Table S5: Data of overdispersion and p0 values from unlogged CAM and unlogged MAM calculation.
- Fig. S5: Relation between CAM D_e and absolute OD.
- Fig. S6: Kernel Density estimate plot of D_e and residual dose distribution.
 - Fig. S7: Mean D_e versus residual dose plot.

Section 4: Associated results of the bleaching experiment

- Fig. S8: Bleaching behaviour of both IR₅₀ and post-IR IRSL₂₀₀ signal.
- Fig: S9: Single-grain bleaching behaviour of CHLEA-3, CHLEA-7, and CHLEA-11.

20 Section 5: Details of microprobe measurement

- Table S6: Measurement details reference material.
- Table S7: Limit of detection of microprobe measurement.
- Fig. S10: Electron backscatter images of single grains.
- Fig. S11: Correlation matrix of residual doses, normalised L_x/T_x values, and all measured oxides.

25 Section 6: Laboratory test of natural dose dependency

- Table S8: Protocol of the laboratory experiment to test natural dose dependency
- Table S9: Summary of residual dose measurements following laboratory irradiation and bleaching
- Fig. S12: Laboratory given dose versus residual dose

Section 7: Lithological composition and luminescence characteristics

30 Fig. S13: Comparison of catchment lithological distribution with mean residual dose and MAM De.

Section 8: Test of recuperation dose as a proxy for bleachability

- Table S10: Statistics of the linear regression fit based on single-grain recuperation dose and residual dose.
- Fig. S14: Relationships between residual dose and recuperation dose.

35 S1: Catchment properties

40

45

50

55

60

To calculate the mean rainfall for each catchment (Table S2), the time-averaged map of daily accumulated precipitation (combined microwave-IR) estimate [GPM_3IMERGDF v06] (Huffman et al., 2023) dataset was utilised. This dataset, spanning the period from January 1, 2001, to December 31, 2019, provides high-resolution precipitation estimates derived from a combination of microwave and infrared measurements. The data was obtained from NASA's Giovanni application, an online tool for accessing and analysing Earth science data. By aggregating daily precipitation values over these 19 years, spatially averaged rainfall data for each catchment were obtained. This approach ensured a robust representation of mean precipitation patterns, accounting for temporal variability and spatial heterogeneity within the study region.

NDVI data were processed using the Google Earth Engine platform (Gorelick et al., 2017). The analysis incorporated Landsat 8 surface reflectance data products from January 2002 to January 2022, with necessary pre-processing involving cloud cover filtering, to calculate the NDVI for each catchment. The JavaScript code available for NDVI calculation from Landsat scenes on the Google Earth Engine tutorials platform was used for this purpose.

Topographic analysis was conducted using a 30 meter resolution Digital Elevation Model (DEM) from the NASA Shuttle Radar Topography Mission (2013). The DEM was further processed using ArcGIS software, which includes filling the sinks, delineating all the catchments (sampling locations were considered as outlets for catchment delineation), and also calculating catchment area, mean slope, and mean elevation.

The Randolph Glacier Inventory-A Dataset of Global Glacier Outlines, Version 7.0 (RGI 7.0 Consortium, 2023) was used to delineate glacier cover within each catchment. This dataset enabled the identification and quantification of glacier coverage, providing essential data for understanding the influence of glacial dynamics on catchment hydrology and geomorphology.

Catchment lithologies were derived from the geological map of South America at a scale of 1:5,000,000 (Gómez et al., 2019). Based on the lithological distribution within each catchment, the major litho-units were classified into four categories: granitic, volcanic, sedimentary, and volcano-sedimentary units, regardless of their age. The proportion of each litho-unit within the catchments (Table S1) was quantified through spatial analysis in ArcGIS software.

Table S1: Details of all eleven samples include sampling location (latitude and longitude), altitude of sampling location, sampling depth, and proportion of the four major lithological units within each catchment. Samples are listed from north to south, CHLEA-11 being the northernmost and CHLEA-5 being the southernmost sample.

Sample ID	Latitude	Longitude	Altitude (m)	Sampling depth (cm)	Granite (%)	Volcanic (%)	Sedimentary (%)	Volcano-sedimentary (%)
CHLEA-11	-28.70	-70.56	656.00	5	67	22	2	9
CHLEA-1	-31.67	-71.29	158.00	20	45	8	10	37
CHLEA-8	-32.85	-70.50	955.00	6	0	28	10	62
CHLEA-6	-33.59	-70.39	861.00	3	0	53	10	37
CHLEA-7	-34.21	-70.53	778.00	11	0	21	19	60
CHLEA-10	-34.68	-70.87	484.00	4	17	0	27	56
CHLEA-3	-35.00	-70.83	633.00	4	0	0	13	87
CHLEA-2	-35.18	-71.12	422.00	3	0	30	5	65
CHLEA-4	-35.73	-71.02	562.00	3	24	9	4	63
CHLEA-9	-36.48	-71.76	275.00	4	2	11	65	22
CHLEA-5	-38.94	-71.92	383.00	7	0	51	49	0

Table S2: Data for each catchment in this study include total catchment area, mean catchment slope, mean catchment elevation, percent glacier-covered area, mean normalised difference vegetation index (NDVI), and daily average rainfall.

Sample ID	Catchment	Total area (km²)	Mean slope (degrees)	Mean elevation (meters)	Glacier area (%)	Mean NDVI	Daily average rainfall (mm)
CHLEA-11	Huasco	7258.37	24.46	3378.99	0.435	0.045	0.34
CHLEA-1	Choapa	5883.15	21.38	2026.08	0	0.085	0.68
CHLEA-8	Aconcagua	2100.09	27.98	3174.8	1.667	0.044	1.17
CHLEA-6	Maipo	4864.59	27.56	3182.09	7.195	0.045	1.86
CHLEA-7	Cachapoal	2411.37	27.43	2680.82	6.612	0.045	2.41
CHLEA-10	Tinguiririca	1838.26	25.58	2328.85	4.225	0.089	2.56
CHLEA-3	Teno	1208.22	26.42	2090.45	0.093	0.102	2.99
CHLEA-2	Lontué	1781.09	19.8	1940.19	0.156	0.125	2.85
CHLEA-4	Maule	2706.2	21.32	2207.62	0.31	0.068	2.68
CHLEA-9	Ñuble	1864.96	22.69	1492.36	0.789	0.21	3.49
CHLEA-5	Allipén	1372.42	17.73	1158.29	3.092	0.281	4.06

S2: Details of preheat plateau and dose recovery test

S2.1: Multi-grain

For multigrain dose-recovery and residual preheat plateau tests, eight aliquots (aliquot size = 2 mm) were bleached for 2 days in the laboratory solar simulator (Sol2) for each preheat temperature examined. Four of these were used for a dose recovery test (given dose: 30 Gy), and the remaining four aliquots were used for measuring the residual dose. Preheat temperatures ranged from 150 °C to 275 °C at intervals of 25 °C. All the measurements were carried out following the protocol outlined in Table S3. All post-IR IRSL measurements at elevated temperatures were performed at 25 °C lower than their corresponding preheat temperature (Table S4).

Over the range of preheat and post-IR IRSL stimulation temperatures tested, dose recovery ratios (DRRs) were calculated for all steps (Fig. S1a). DRRs were determined after subtracting the average residual dose from the average measured dose of all accepted aliquots, following the acceptance criteria outlined in Section 2.3 of the main text. All the post-IR IRSL signals produced good dose recovery results. Among them, the DRR for the post-IR IRSL₂₀₀ signal (with the preheat temperature of 225 °C) yielded the best result for both samples. The post-IR IRSL₂₀₀ DRRs for CHLEA-11 and CHLEA-6 were 0.98 ± 0.05 and 0.98 ± 0.06 respectively, well within the range of 0.90 to 1.10 (unity $\pm 10\%$). Thus, the post-IR IRSL₂₀₀ signal was selected for further analysis.

S2.2: Single-grain

Once the protocol was established using multi-grain aliquots, individual K-feldspar grains were loaded into single-grain discs with 300 μ m holes to perform a dose recovery test, assessing the suitability of the protocol at the single-grain level on four samples (CHLEA-11, CHLEA-6, CHLEA-10, and CHLEA-9). The protocol described in Table S3 (for single-grain) was used for post-IR IRSL₂₀₀ signal measurement and analysis. Grains were bleached for 2 days in the Sol2 prior to measurement. 5 to 16 single-grain discs (equivalent to 500 to 1600 grains) were measured for both residual dose measurement and dose recovery tests (given dose: 30 Gy). The residual subtracted DRRs of the four samples were 0.87 \pm 0.02, 0.88 \pm 0.06, 0.93 \pm 0.06, and 0.84 \pm 0.07 respectively (Fig. S2).

110

105

Table S3: Post-IR IRSL measurement protocol of dose recovery and residual preheat plateau test on multigrain aliquots and single-grain (SG) dose recovery tests. ^aFor the dose recovery test, the given dose was 30 Gy with regenerative doses of 0, 10, 20, 30, and 50 Gy and a ^ctest dose of 20 Gy. ^bFor residual dose measurement, regenerative doses of 0, 2, 5, 10, and 30 Gy were applied, with a ^ctest dose of 10 Gy. The range of preheat temperatures used was X = 150, 175, 200, 225, 250, and 275. The post-IR IRSL stimulation temperature was always 25 °C lower than the applied preheat temperature (i.e., X-25). Post-IR IRSL₂₀₀ was measured for the single-grain dose recovery test.

Step	Treatment	Observed
1	Beta dose ^{a,b}	
2	Preheat X °C, 60 s	
3	IRSL 50 °C, 200 s (2 s for SG)	
4	post-IR IRSL at (X-25) °C, 300 s (3 s for SG)	L_{x}
5	Test dose ^c	
6	Preheat X °C, 60 s	
7	IRSL 50 °C, 200 s (2 s for SG)	
8	post-IR IRSL at (X-25) °C, 300 s (3 s for SG)	T_x
9	Repeat steps 1 to 8 for a range of regenerative doses (incl. zero and repe	eat
	dose, zero dose measured after the largest regenerative dose)	

Table S4: Preheat and post-IR IRSL stimulation temperature combinations of multi-grain dose recovery and residual preheat plateau test.

Preheat stimulation temperature (°C)	Post-IR IRSL stimulation temperature (°C)
150	125
175	150
200	175
225	200
250	225
275	250

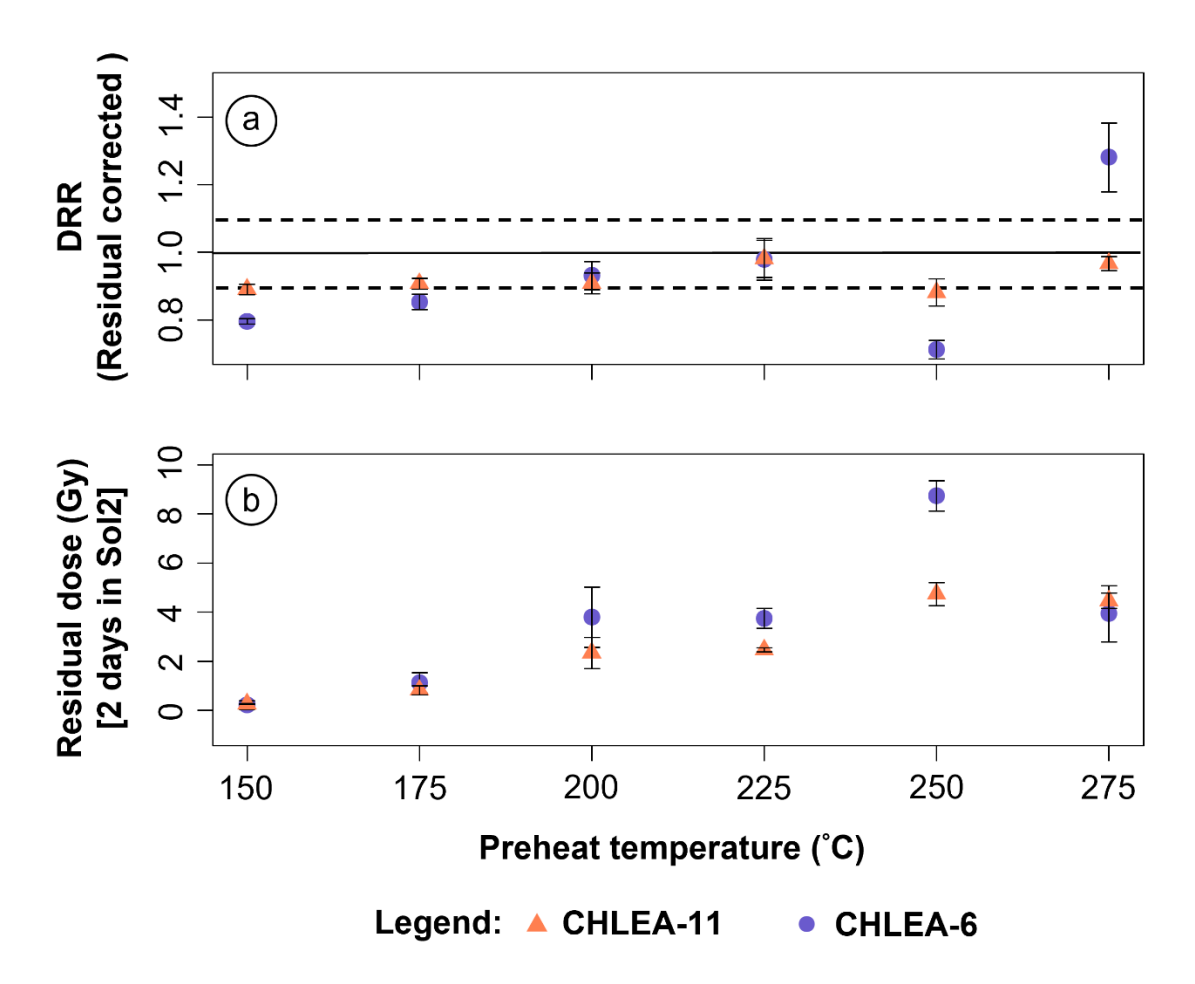


Fig. S1: Results of the dose recovery and residual preheat plateau test performed on samples CHLEA-11 and CHLEA-6 using multi-grain aliquots. (a) Residual corrected dose recovery ratios (DRRs) and (b) residual dose (Gy) estimates, calculated at each preheat temperature. Each data point on both plots represents the average of accepted aliquots. Note that post-IR IRSL stimulation temperature was always 25 °C lower than the applied preheat stimulation temperature. All uncertainties are indicated as one standard error.

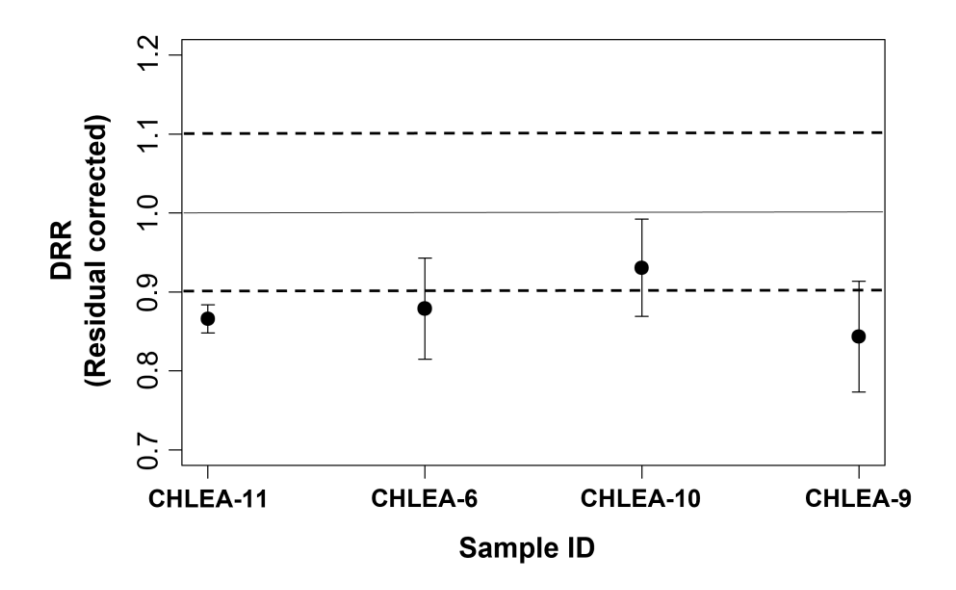


Fig. S2: Residual corrected dose recovery ratios (DRRs) of samples CHLEA-11, CHLEA-6, CHLEA-10, and CHLEA-9 performed at the single-grain level. All uncertainties are indicated as one standard error.

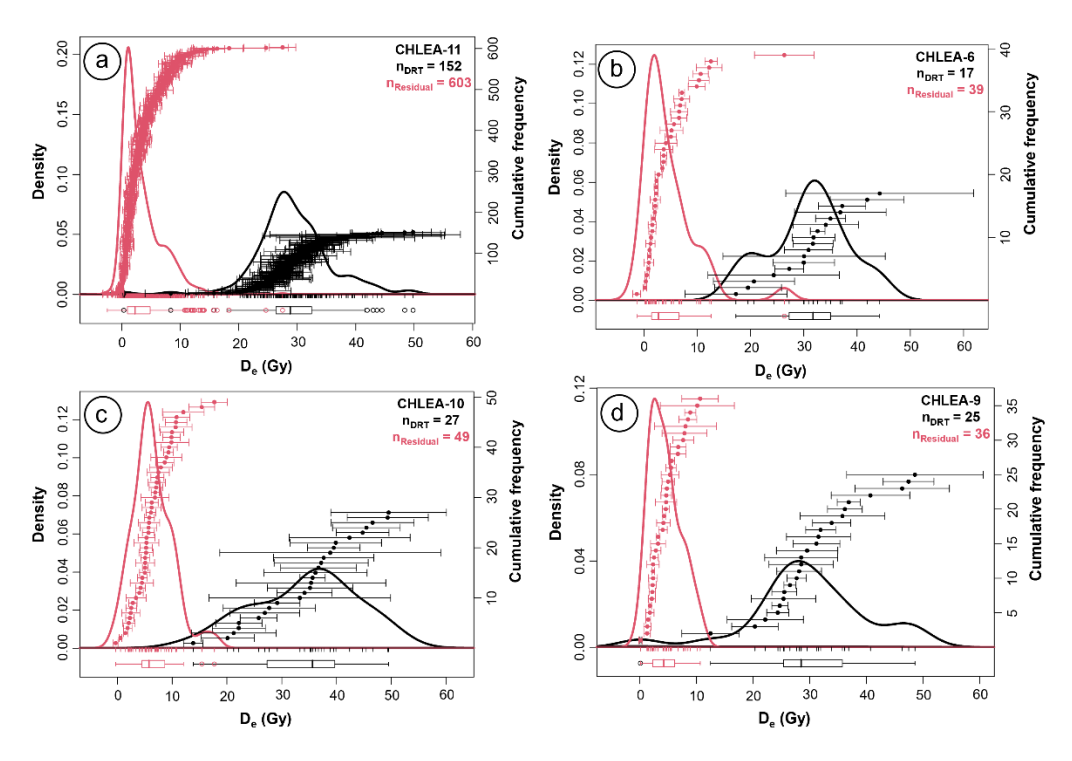


Fig. S3: Kernel density estimate plot of all four samples subjected to single-grain dose recovery test and corresponding residual dose measurement. plot_KDE() (Dietze, M., 2023) function of the R-Luminescence package was used to make plots of kernel density estimates shown here. In all panels, ndr and nresidual represent the number of grains accepted from the dose recovery test and residual dose measurement, respectively.

S3: Details of ancillary luminescence data

S3.1: Luminescence decay and dose response curves

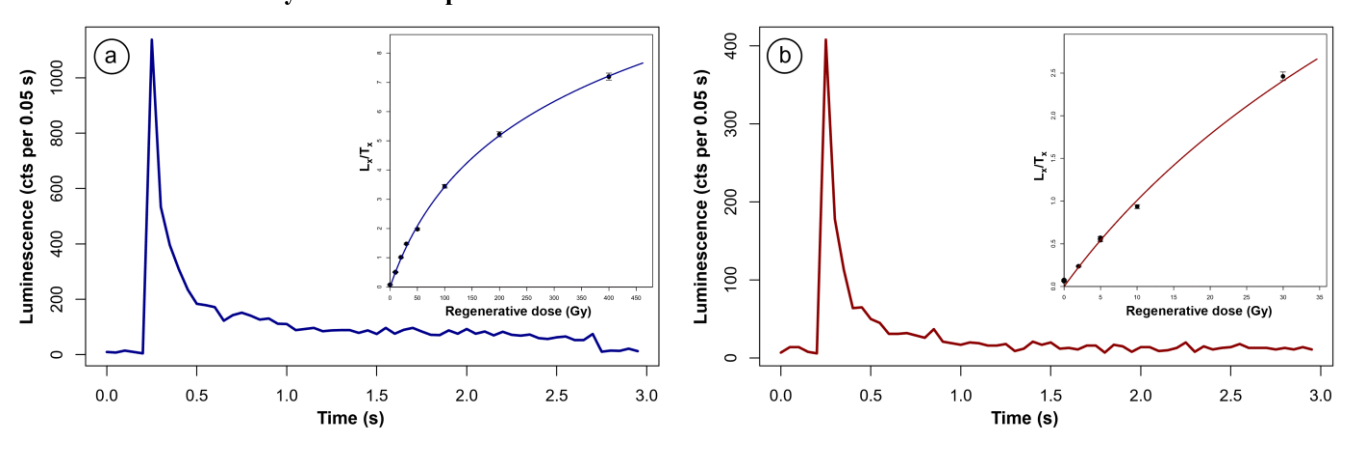


Fig. S4: Examples of single-grain luminescence decay curves and dose response curves of post-IR IRSL $_{200}$ signal from equivalent dose (a) and residual dose (b) measurement. The net post-IR IRSL $_{200}$ signal was calculated from the signal integrated over the first 0.25 s (from the initial part of the decay curve) with subtraction of the background estimated from the last 0.50 s.

S3.2: CAM and MAM data

140

145

150

calc_CentralDose() (Burow, C., 2023) function of the R-Luminescence package (Kreutzer et al., 2023) was used to calculate unlogged central age model equivalent dose and associated derivatives like absolute overdispersion (OD), relative OD (%). calc_MinDose() (Burow, C., 2023) function was used to calculate unlogged minimum age model equivalent dose and associated derivative, like p0 value.

Table S5: Details of absolute and relative overdispersion (OD) calculated for all samples using the unlogged central age model (CAM). Also, the p0 (representing the proportion of well-bleached grains included in the equivalent dose estimation) value from the 3-parameter unlogged minimum age model (MAM).

Sample ID	CAM OD (Gy)	CAM OD (%)	MAM p0
CHLEA-11	15.4 ± 0.6	99.5 ± 7.1	0.89
CHLEA-1	43.6 ± 3.1	151.6 ± 25.1	0.72
CHLEA-8	29.0 ± 3.1	126.6 ± 27.4	0.7
CHLEA-6	35.2 ± 3.1	93.0 ± 13.1	0.4
CHLEA-7	37.9 ± 1.8	74.8 ± 5.0	0.43
CHLEA-10	18.3 ± 1.8	70.0 ± 9.3	0.64
CHLEA-3	42.8 ± 3.8	103.3 ± 16.0	0.59
CHLEA-2	42.2 ± 3.7	122.7 ± 21.0	0.54
CHLEA-4	17.5 ± 1.6	109.8 ± 18.7	0.65
CHLEA-9	31.1 ± 3.0	102.5 ± 16.9	0.53

CHLEA-5 24.5 ± 2.3 109.6 ± 19.1 0.67

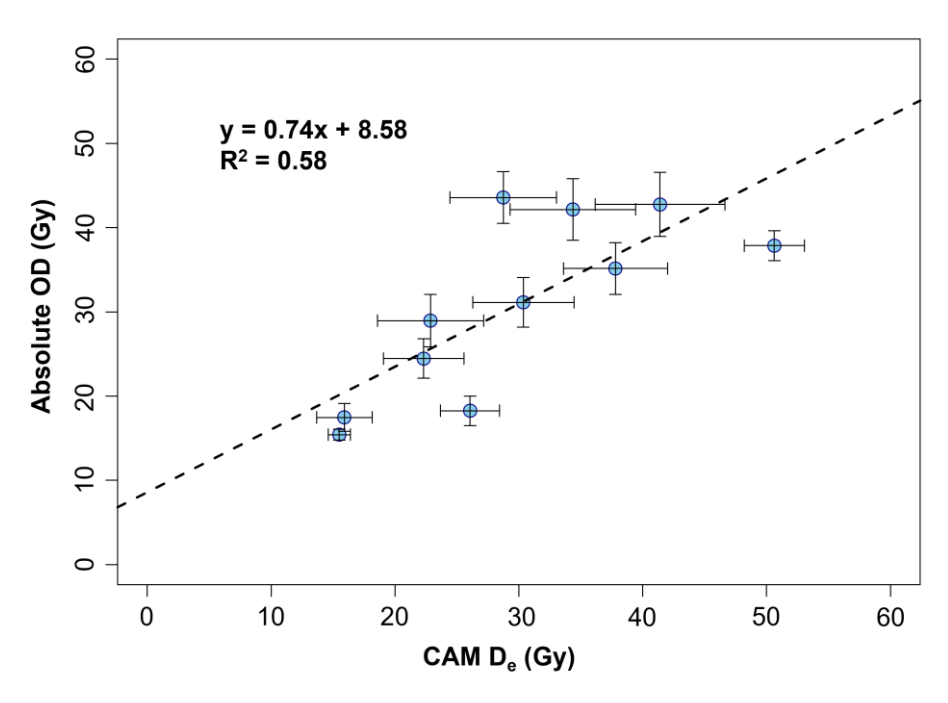


Fig. S5: Linear relation between CAM D_e (Gy) and absolute OD (Gy). Both of these values were obtained for all samples using an unlogged central age model (CAM). Note the intercept of the linear fit on the Y-axis. This intercept (8.58 Gy) was used as the sigma-b (overdispersion) value while calculating the equivalent dose by applying the unlogged minimum age model for all samples.

S3.3: KDE plots of De and residual dose distribution

Figure S6 presents kernel density estimate plots of single-grain equivalent dose (D_e) and residual dose estimates for some selected samples. Panels (a) and (c) display data for CHLEA-4 and CHLEA-7, respectively, while panels (b) and (d) correspond to CHLEA-6 and CHLEA-9. Despite CHLEA-4 and CHLEA-7 originating from catchments with similar dominant lithology (Table S1), their D_e (unlogged-MAM) and residual dose estimates differ markedly (Table 3, main text). In contrast, CHLEA-6 and CHLEA-9 exhibit comparable D_e (unlogged-MAM) and residual dose estimates, despite different dominant lithologies (Table S1).

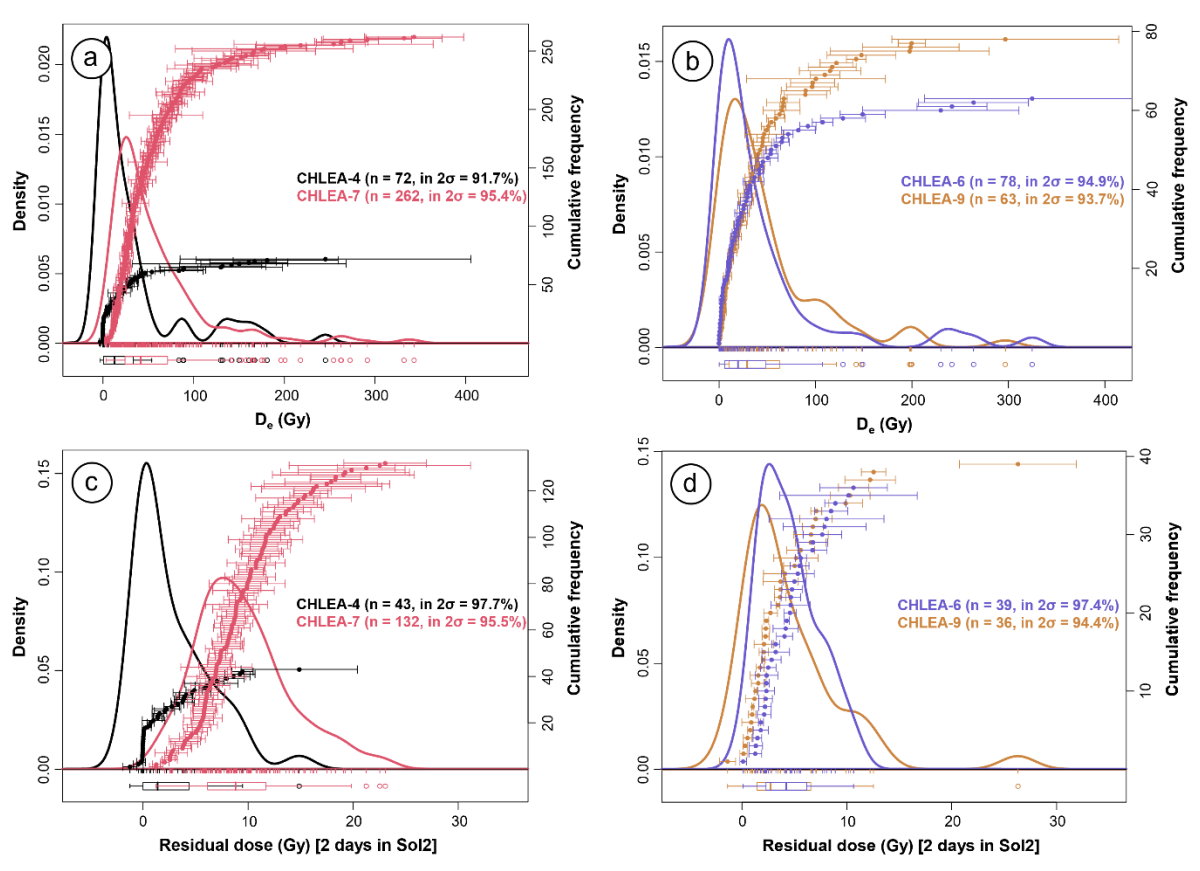


Fig. S6: Examples of kernel density estimate plots of single-grain equivalent dose (D_e) estimates and residual dose estimates for samples CHLEA-4 and CHLEA-7 in panels (a) and (c), respectively; and for samples CHLEA-6 and CHLEA-9 in panels (b) and (d), respectively. plot_KDE() (Dietze, M., 2023) function of the R-Luminescence package was used to make plots of kernel density estimates shown here.

S3.4: Mean De versus mean residual dose

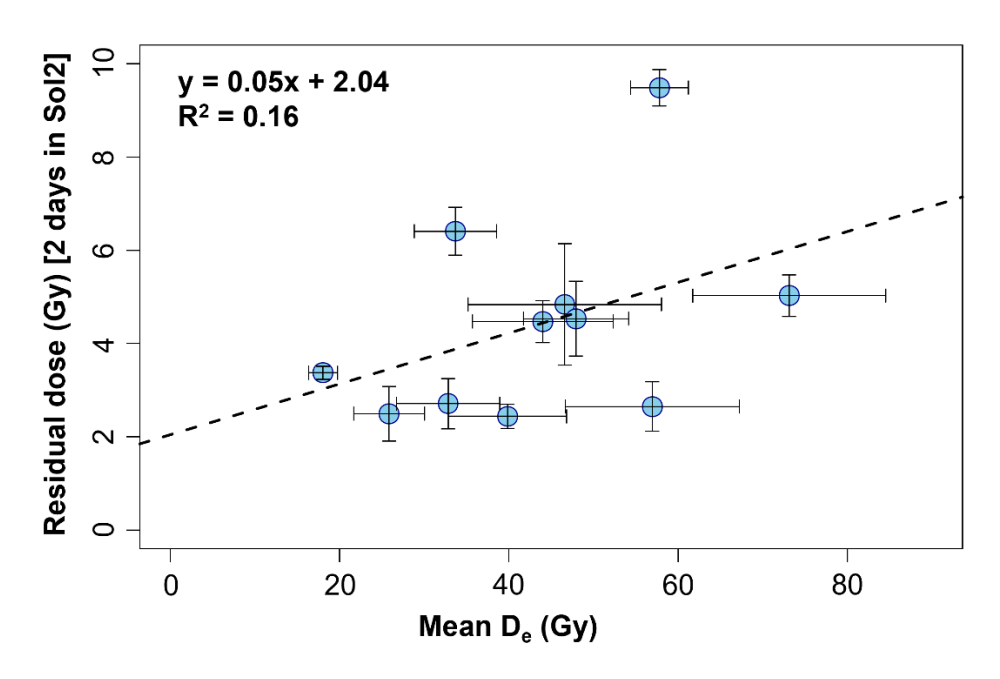
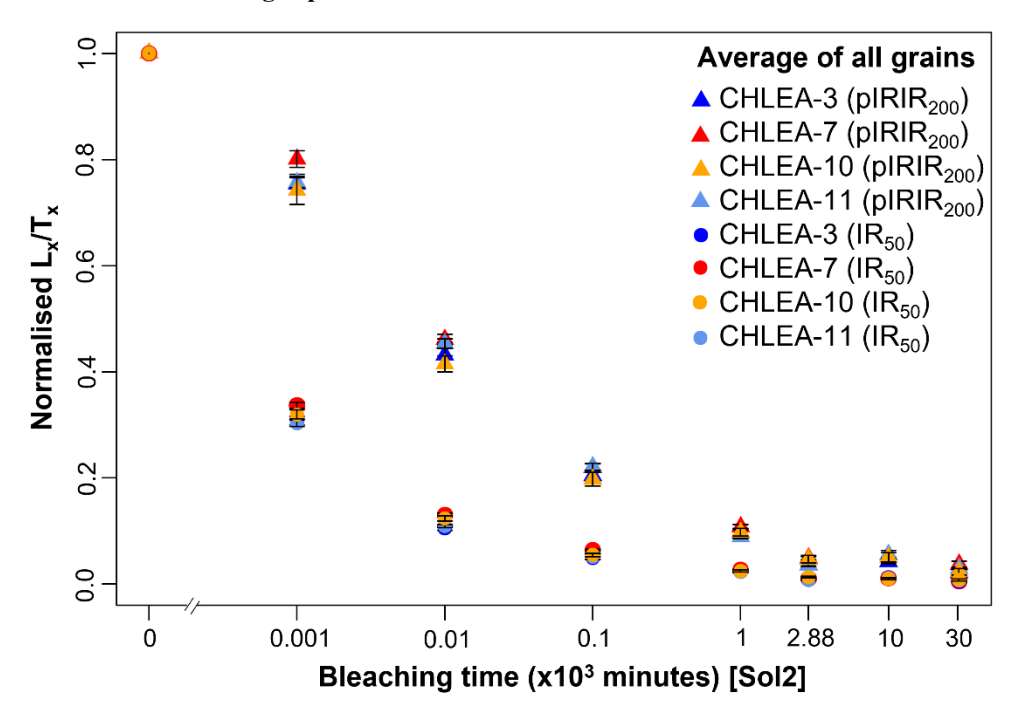


Fig. S7: Mean De versus mean residual dose with a linear fit, fitting equation, and coefficient of correlation.

195 S4: Associated results of the bleaching experiment



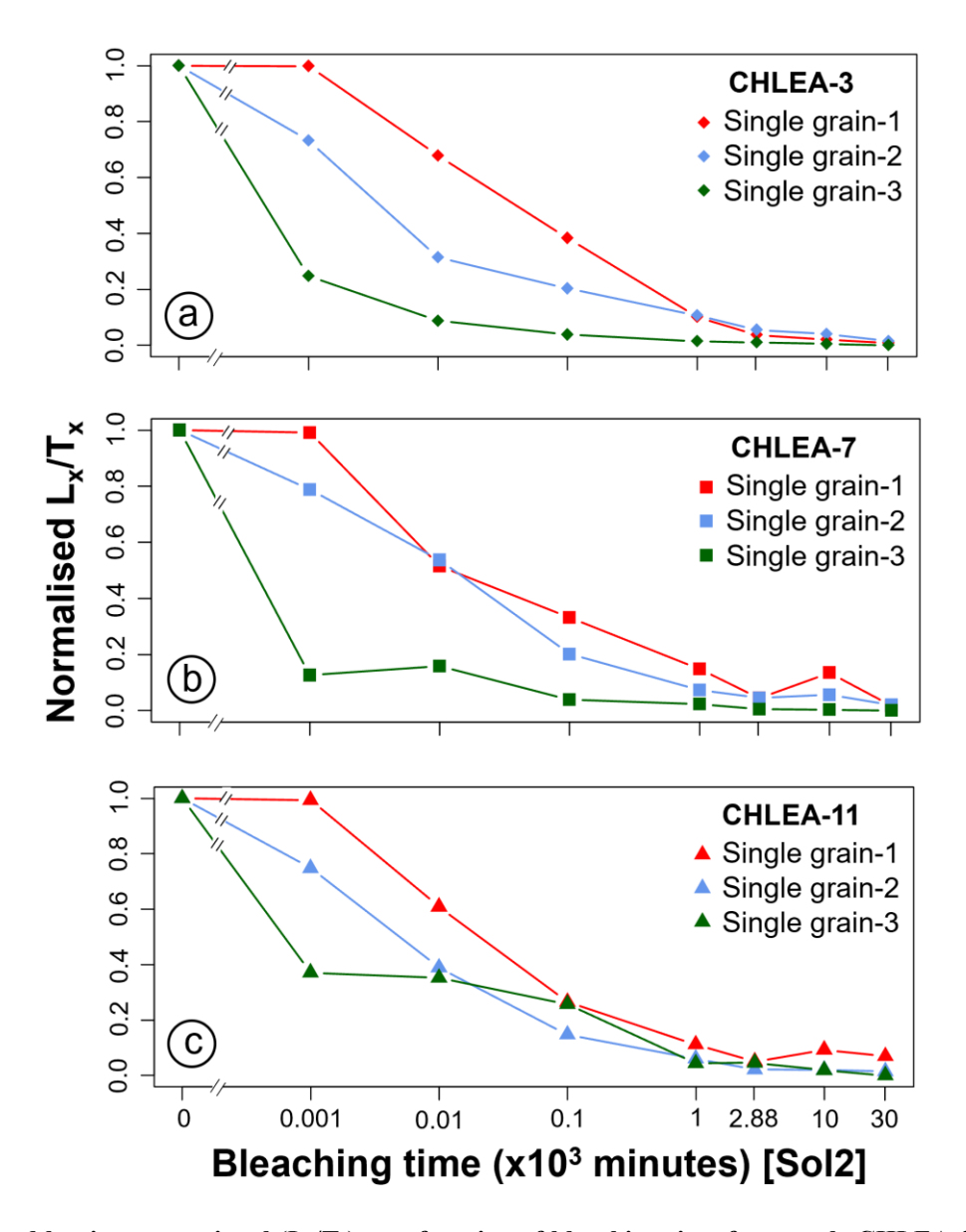


Fig. S9: Normalised luminescence signal (L_x/T_x) as a function of bleaching time for sample CHLEA-3 (a), CHLEA-7 (b), and CHLEA-11 (c), illustrating bleachability of the post-IR IRSL₂₀₀ signal at the single-grain level. Each panel presents three representative grains selected based on their initial bleaching rates: fast, medium, and slow, determined after 1 minute of Sol2 exposure. The data highlight the variability in bleaching rates and behaviours among individual grains over time (Uncertainties are not displayed).

S5: Details of microprobe measurement

Over three measurement days, concentrations of all major elements (>1 wt%) remained within 5% of the reference composition for the P&H orthoclase secondary standard, except BaO, which stayed within 10%. Fe₂O₃ and CaO deviated by more than 10%, and their results should be interpreted with caution. The microprobe data were filtered based on the minimum detection limits of K₂O (0.03 wt%) and Na₂O (0.04 wt%), the two key elements involved in the solid-solution relationships among various feldspar phases observed in our samples (Fig. S10a–d). MnO concentrations were below the microprobe's detection limit and were therefore excluded from all analyses. Additionally, filtering was performed to exclude erroneous measurements of major oxide concentrations in K-feldspar grains where the total concentration (wt%) fell outside the range of 100 ± 5 wt%.

Table S6: Measurement details of orthoclase from the P&H standard block as secondary reference material before and after each measurement session to monitor precision and accuracy. The results indicate the mean (± 2 standard deviations) of ten (five before and five after each measurement session) measurement points.

Measurement	Reference	Fe ₂ O ₃	Na ₂ O	K ₂ O	BaO	MnO	SiO ₂	CaO	Al ₂ O ₃	Total
date	material	(wt%)	(wt%)	(wt%)	(wt%)	(wt%)	(wt%)	(wt%)	(wt%)	(wt%)
16.12.2024	P&H orthoclase	0.024 ± 0.05	1.4 ± 0.4	14.7 ± 0.5	0.1 ± 0.1	0.01 ± 0.03	64.2 ± 0.8	0.016 ± 0.032	18.8 ± 0.4	99 ± 1
17.12.2024	P&H orthoclase	0.02 ± 0.042	1.4 ± 0.1	14.5 ± 0.3	0.14 ± 0.07	0.01 ± 0.02	65 ± 1	0.017 ± 0.029	18.7 ± 0.5	100 ± 2
18.12.2024	P&H orthoclase	0.031 ± 0.065	1.4 ± 0.2	14.5 ± 0.3	0.16 ± 0.05	0.01 ± 0.05	65 ± 2	0.013 ± 0.025	18.8 ± 0.7	100 ± 2

Table \$7. Limit of detection of microprobe measurements

Oxides	Fe ₂ O ₃	Na ₂ O	K ₂ O	BaO	MnO	SiO ₂	CaO	Al ₂ O ₃
Limit of detection (wt%)	0.058	0.04	0.03	0.092	0.05	0.04	0.027	0.04

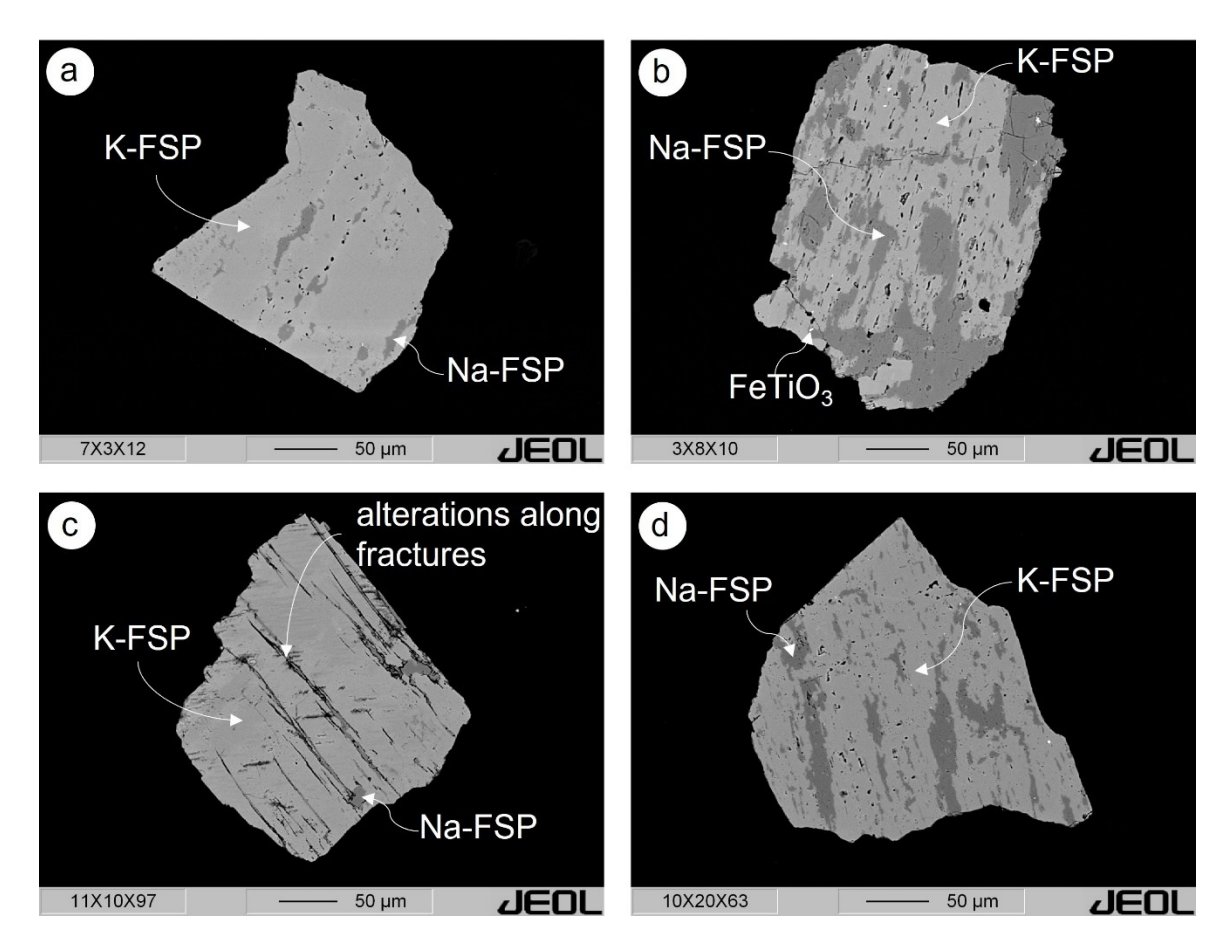


Fig. S10: Electron back scatter images of four selected grains (a-d), one from each sample subjected to the bleaching experiment. Images were captured and the mineralogical composition indicated in the images is based on energy-dispersive X-ray spectroscopy (EDS) analysis performed during microprobe measurement. Na-FSP: Na-feldspar and K-FSP: K-feldspar. Note the alterations present along the fractures (panel c). The number combination at the bottom left of each figure shows the sample number, disc number and the measured grain number. For example, in (a) 7X3X12 means grain number 12 from disc 3 of sample CHLEA-7.

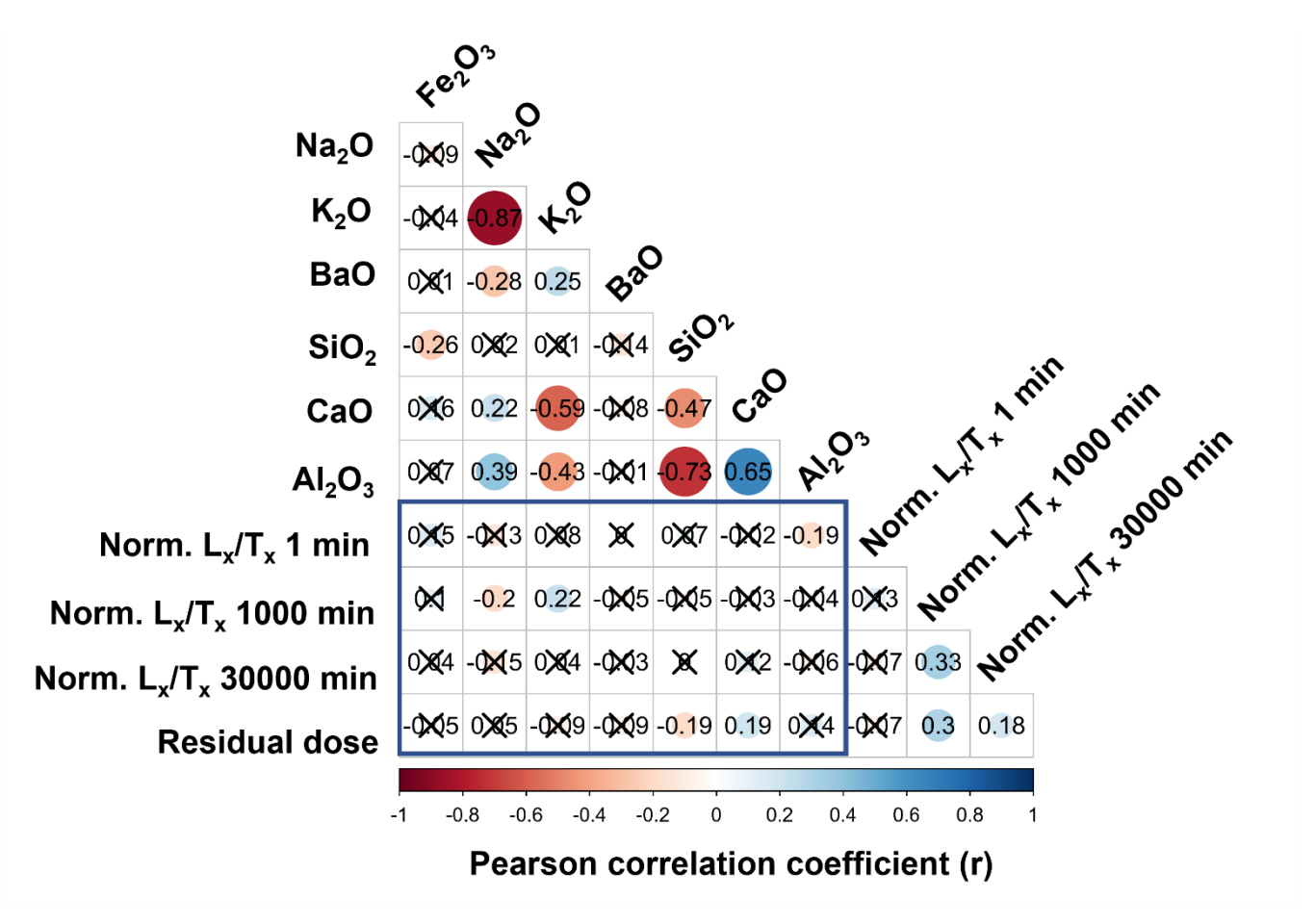


Fig. S11: Correlation matrix showing the correlation between and within grain-specific residual dose (measured dose after 2 days of Sol2 bleaching), normalised L_x/T_x of 1 minute, 1000 minutes, and 30000 minutes bleaching steps and all measured oxides for all four samples subjected to the bleaching experiment. Numbers in the circles represent Pearson correlation coefficient (r) values, and size and colour show the strength of the correlation. The boxes with cross marks represent statistically non-significant correlations with a p-value greater than 0.05. The blue rectangle in the figure marks the correlation between geochemical data and luminescence data.

Section 6: Laboratory test of natural dose dependency

Table S8: Protocol of the laboratory experiment to test natural dose dependency.

Steps	Actions
1	Dose (0, 30, 60, 120 Gy) above the respective natural doses
2	2 days of bleaching in Sol2
3	Residual dose measurement following the protocol in Table 1

250

Table S9: Summary of residual dose measurements for samples CHLEA-7 and CHLEA-11 following laboratory-given dose and subsequent bleaching under Sol2. n (%): absolute and relative number of accepted residual dose grains. All uncertainties indicate one standard error.

Sample ID	Given dose (Gy)	n (%)	Mean residual dose (Gy)
CHLEA-7	0	132 (33)	9.5 ± 0.4
	30	123 (41)	8.5 ± 0.3
	60	122 (41)	8.7 ± 0.3
	120	119 (40)	8.4 ± 0.3
CHLEA-11	0	603 (38)	3.4 ± 0.1
	30	152 (51)	3.1 ± 0.2
	60	142 (47)	3.2 ± 0.2
	120	131 (44)	3.7 ± 0.3

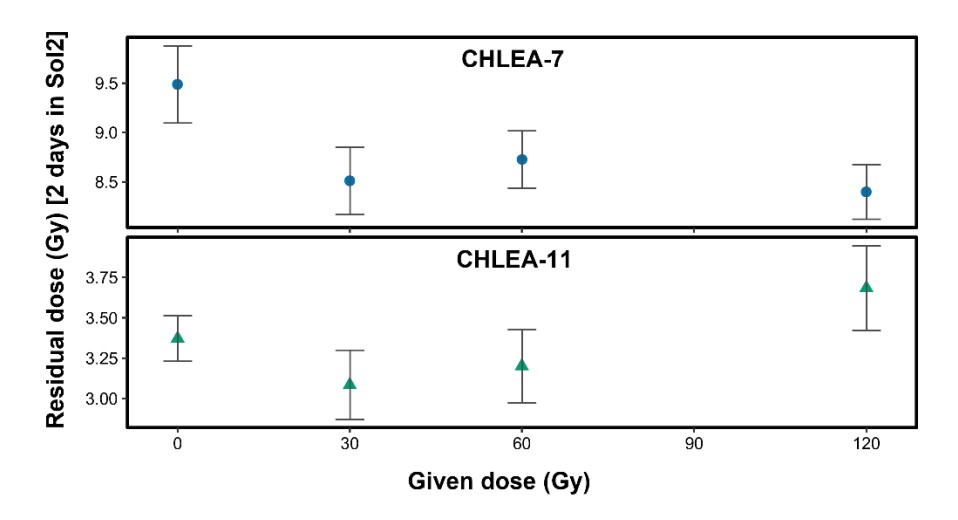


Fig S12: Average residual dose measured following irradiation with additional doses of 30, 60, and 120 Gy above the respective natural doses, followed by a 2-day bleaching period under Sol2. Each data point represents the mean of single-grain measurements (Table S7) obtained from three individual single-grain discs, except for the 0 Gy dose point, which utilizes residual dose values reported in Table 3. Error bars denote ±1 standard error.

Section 7: Lithological composition and luminescence characteristics

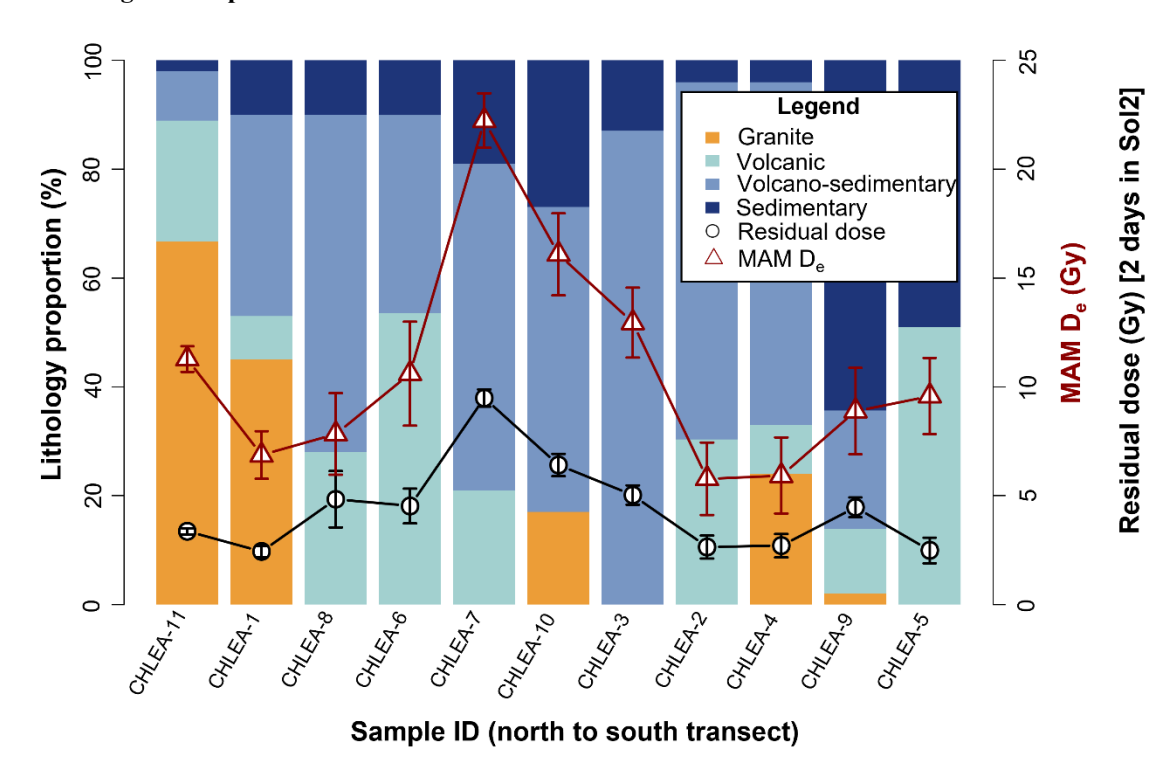


Fig S13: Lithological composition and luminescence characteristics of all eleven catchments in the Southern Central Andes, Chile. Stacked bars show the relative proportions (%) of four lithological categories: Granite, Volcanic, Volcano-sedimentary, and Sedimentary, within each catchment. Superimposed symbols indicate luminescence signal properties: black circles represent the residual dose (measured after 2 days of bleaching in Sol2), while red triangles indicate the unlogged minimum age model equivalent dose (MAM D_e) for each sample. Uncertainties indicate one standard error. Sample IDs (CHLEA) are ordered geographically from north to south.

Section 8: Test of recuperation dose as a proxy for bleachability

285

290

Residual doses of individual grains were compared with their corresponding recuperation doses, which were derived from measurements conducted within the single aliquot regenerative dose (SAR) protocol (Table 1, Step 10: zero-dose measurement following the natural signal). To estimate the recuperation dose, the test dose corrected luminescence response was projected onto the linear segment of the dose-response curve, defined between the origin and the response to the third regenerative dose (~5 Gy). Associated uncertainties were propagated based on the errors of individual measurements.

A subset of recuperation doses yielded negative values, which are interpreted as artifacts likely arising from elevated background-to-signal ratios. To keep the analysis physically meaningful, only positive recuperation dose values were considered. To evaluate the potential of recuperation dose as an indicator of grain-specific bleachability, we conducted a weighted regression analysis between recuperation dose and residual dose. The results of this analysis are summarised in Table S8.

Table S10: Summary statistics of the weighted linear regression fit based on single-grain recuperation dose and residual dose. Note that the n represents the number of positive data points used in the weighted linear regression.

Sample ID	n	Intercept	Slope	Adjusted R ²	p-value
CHLEA-11	534	1.00	0.11	0.00	0.38
CHLEA-1	74	0.35	1.65	0.11	0.00
CHLEA-8	14	2.96	-0.94	-0.04	0.51
CHLEA-6	31	0.62	2.64	0.32	0.00
CHLEA-7	123	3.98	3.50	0.17	0.00
CHLEA-10	39	1.25	4.10	0.35	0.00
CHLEA-3	54	-0.52	2.27	0.07	0.03
CHLEA-2	44	-0.07	0.65	0.07	0.04
CHLEA-4	24	0.08	-0.04	-0.04	0.90
CHLEA-9	28	2.76	0.03	-0.04	0.98
CHLEA-5	23	-0.78	4.49	0.46	0.00

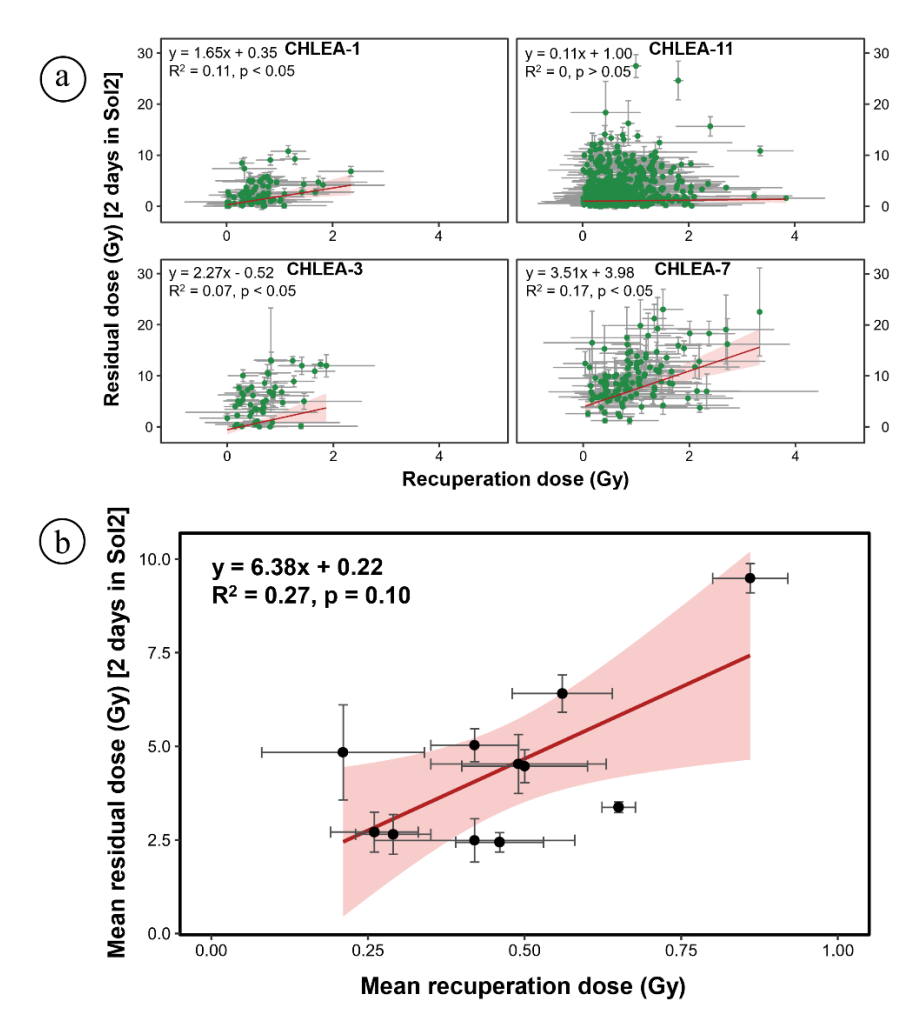


Fig S14: Relationships between residual dose and recuperation dose. (a) Scatter plots showing residual dose versus recuperation dose at single-grain level for four samples (CHLEA-1, CHLEA-11, CHLEA-3, CHLEA-7). Each panel includes the statistics (regression equation, R², and p-value) of the fitted linear regression. (b) Sample-averaged residual dose plotted against sample-averaged recuperation dose, with linear regression. The shaded red envelope around the regression line represents a 95% confidence interval. Error bars represent ±1 standard error.

References

295

Burow, C., 2023. calc_CentralDose(): Apply the central age model (CAM) after Galbraith et al. (1999) to a given De distribution. Function version 1.4.1. In: Kreutzer, S., Burow, C., Dietze, M., Fuchs, M.C., Schmidt, C., Fischer, M., Friedrich, J., Mercier, N., Philippe, A., Riedesel, S., Autzen, M., Mittelstrass, D., Gray, H.J., Galharret, J., 2023. Luminescence: Comprehensive Luminescence Dating Data Analysis. R package version 0.9.21, https://CRAN.R-project.org/package=Luminescence

- Burow, C., 2023. calc_MinDose(): Apply the (un-)logged minimum age model (MAM) after Galbraith et al. (1999) to a given De distribution. Function version 0.4.4. In: Kreutzer, S., Burow, C., Dietze, M., Fuchs, M.C., Schmidt, C., Fischer, M., Friedrich, J., Mercier, N., Philippe, A., Riedesel, S., Autzen, M., Mittelstrass, D., Gray, H.J., Galharret, J., 2023. Luminescence: Comprehensive Luminescence Dating Data Analysis. R package version 0.9.21, https://CRAN.R-project.org/package=Luminescence
- Carretier, S., Regard, V., Vassallo, R., Aguilar, G., Martinod, J., Riquelme, R., Pepin, E., Charrier, R., Herail, G., Farias, M., Guyot, J.L., Vargas, C., and Lagane, C.: Slope and climate variability control of erosion in the Andes of central Chile, Geology, 41(2), 195-198. https://doi.org/10.1130/G33735.1, 2013.
 Dietze, M., 2023. plot_KDE(): Plot kernel density estimate with statistics. Function version 3.6.0. In: Kreutzer, S., Burow, C., Dietze, M., Fuchs, M.C., Schmidt, C., Fischer, M., Friedrich, J., Mercier, N., Philippe, A., Riedesel, S., Autzen, M.,
- Mittelstrass, D., Gray, H.J., Galharret, J., 2023. Luminescence: Comprehensive Luminescence Dating Data Analysis. R package version 0.9.21, https://CRAN.R-project.org/package=Luminescence
 Gómez, J., Schobbenhaus, C., and Montes, N.E.: Geological Map of South America 2019. Scale 1:5 000000. Commission for the Geological Map of the World (CGMW), Servicio Geológico Colombiano and ServiçoGeológico do Brasil. Paris, France, https://doi.org/10.32685/10.143.2019.929, 2019.
- Gorelick, N., Hancher, M., Dixon, M., Ilyushchenko, S., Thau, D., and Moore, R.: Google Earth Engine: Planetary-scale geospatial analysis for everyone, Remote Sens. Env., 202, 18-27, https://doi.org/10.1016/j.rse.2017.06.031, 2017.
 Huffman, G.J., E.F. Stocker, D.T. Bolvin, E.J. Nelkin, Jackson Tan (2023), GPM IMERG Final Precipitation L3 1 day 0.1 degree x 0.1 degree V06, Edited by Andrey Savtchenko, Greenbelt, MD, Goddard Earth Sciences Data and Information Services Center (GES DISC), Accessed: 2023-05-17, 10.5067/GPM/IMERGDF/DAY/06
- Kreutzer, S., Burow, C., Dietze, M., Fuchs, M.C., Schmidt, C., Fischer, M., Friedrich, J., Mercier, N., Philippe, A., Riedesel, S., Autzen, M., Mittelstrass, D., Gray, H.J., and Galharret, J.: Luminescence: Comprehensive Luminescence Dating Data Analysis, R package version 0.9.23, https://CRAN.R-project.org/package=Luminescence, 2023.
 NASA Shuttle Radar Topography Mission (SRTM) (2013). Shuttle Radar Topography Mission (SRTM) Global. Distributed by OpenTopography, https://doi.org/10.5069/G9445JDF. Accessed: 2023-05-01.
- Pepin, E., Carretier, S., Guyot, J. L., and Escobar, F.: Specific suspended sediment yields of the Andean rivers of Chile and their relationship to climate, slope and vegetation, Hydrol. Sci. J., 55(7), 1190-1205, https://doi.org/10.1080/02626667.2010.512868, 2010.
 RGI 7.0 Consortium, 2023. Randolph Glacier Inventory A Dataset of Global Glacier Outlines, Version 7.0. Boulder,
- 340 https://doi.org/10.5067/f6jmovy5navz

Colorado USA. NSIDC: National Snow and Ice Data Center. doi:10.5067/f6jmovy5navz. Online access: